arXiv:1612.06135v1 [cond-mat.str-el] 19 Dec 2016

Raman anomalies as signatures of pressure induced electronic topological and structural transitions in black phosphorus: Experiments and Theory

Satyendra Nath Gupta[1], Anjali Singh[2], Koushik Pal[2], Biswanath Chakraborty[1], D.V.S.Muthu[1], U V Waghmare[2] and A. K. Sood[1*]
[1]*Department of Physics, Indian Institute of Science, Bangalore-560012,India* [2]*Theoretical Sciences Unit, Jawaharlal Nehru Centre for Advanced Scientific Research, Bangalore-560064, India*

(Dated: December 20, 2016)

We report high pressure Raman experiments of Black phosphorus (BP) up to 24 GPa. The line widths of first order Raman modes A_g^1, B_{2g} and A_g^2 of the orthorhombic phase show a minimum at 1.1 GPa. Our first-principles density functional analysis reveals that this is associated with the anomalies in electron-phonon coupling at the semiconductor to topological insulator transition through inversion of valence and conduction bands marking a change from trivial to nontrivial electronic topology. The frequencies of B_{2g} and A_g^2 modes become anomalous in the rhombohedral phase at 7.4 GPa, and new modes appearing in the rhombohedral phase show anomalous softening with pressure. This is shown to originate from unusual structural evolution of black phosphorous with pressure, based on first-principles theoretical analysis.

PACS numbers: 78.30.-j, 71.30.+h, 71.15.Mb

I. INTRODUCTION

The Black phosphorus (BP) is the most stable form among the many allotropic modifications of phosphorus at room temperature and ambient pressure. It is an elemental semiconductor with direct band gap of ∼0.3 eV. Recently there is revival of interest in BP from the prospective of a layered material which allows us to study the exciting properties of a mono and few layers of BP[1–8]. It is found that the band gap depends on the thickness of its film: 0.3eV for thickness $> 4nm$ and 1.2 eV for single layer thick BP[9]. This moderate band gap bridges the gap between the semimetallic graphene[10,11] and relatively large band gap of transition metal dichalcogenide (1.5-2.5eV)[12–14] and makes it ideal for infrared optoelectronic application. Another interesting feature of BP is its anisotropic atomic structure. At ambient pressure, BP packs into orthorhombic lattice with a puckered honeycomb structure as shown in Fig. 1. Each phosphorus atom is bonded with two in plane and one out of plane neighboring atoms. The puckered layers are bound together by weak van der Waals interactions. Due to this anisotropic atomic structure, the effective masses of carriers in BP along arm chair (ac) are lightest and that along the layer stacking (z) are lighter than that along the zigzag (zz)[15]. Recent upsurge of interest in layered BP has arisen due to this unique puckered 2-D honeycomb lattice in each phosphorus layer, giving anisotropic electronic[8], optical[4,8] and vibrational properties[4].

Further, the direct band gap ($\sim 0.3eV$) of BP arises from the out-of-plane p_z-like orbitals of phosphorus and hence can be strongly modulated by pressure or c-axis strain. Not surprisingly, the effect of pressure was studied on crystal structure and electronic properties in the early work[16–22]. It has anisotropic compressibility: lattice parameters a and c decrease more in comparison with the lattice parameter b with increasing pressure. At room temperature, the ambient pressure orthorhombic structure transforms to the rhombohedral structure at P_{c2} ∼4.7 GPa and then to the simple cubic structure (sc) at $P_{c3} \sim 11$ GPa[22]. These transition pressures are slightly higher if sample is cooled to liquid helium temperature first and then pressure is increased. The sc phase transforms to a simple hexagonal (sh) phase at higher pressure 137 GPa via an intermediate phase[23]. Recently, Akahama et. al[24] investigated the crystal structure of black phosphorus up to 280 GPa at room temperature using x-ray-diffraction experiment and found that sh phase goes to the bcc structure at 262 GPa. The sc phase exhibits superconductivity at 4.7 K[25,26]. The superconducting temperature is slightly pressure dependent and increases with increasing pressure. The superconducting state remains for several hours even if the pressure is removed. BP shows superconductivity with high transition temperature (10K) when it is cooled to 4K first and then pressure is applied. These experiments clearly establish that high pressure can be used to tune the material characteristic of BP significantly.

The electrical conductivity of black P is also very sensitive to pressure[27–29]. Two anomalies have been reported at 1.7 and 4.2 GPa, the latter coinciding with the structural phase transition from orthorhombic to rhombohedral structure. The earlier work[30] reported that the band gap decreased linearly with a pressure coefficient of $\sim$ 0.17 eV/ GPa, closing at $P_{c1} \sim 1.5$ GPa. Recent magneto-resistance studies[31] have termed this transition as electronic topological transition (ETT) from semiconductor to 3D Dirc semi-metal due to band crossover near the Z-point in the Brillouin zone with linear dispersion. Interestingly, a colossal magneto-resistance of $\sim 80,000$ is seen at 2GPa at a field of 9T, similar to 2D Weyl semimetals like WTe_2, making BP as an elemental semi-metal with increased electronic structure.

Pressure and strain have been used to change the rela-

tive strength of spin-orbit coupling and induce electronic topological transition (ETT) in materials like Sb_2Se_3[32], b-As_2Te_3[33], BiTeI[34]. Recently, Gong et al.[35] theoretically reported a pressure-induced Lifshitz transition at a pressure of 1.23 GPa where black phosphorus undergoes a semiconductor to three-dimensional Dirac semimetal transition. By using first-principles density functional theoretical calculations within GGA and mBJ exchange-correlation functional, Gong et al.[35] showed that the band inversion occurs at the Z point at 1.23 GPa and robust three-dimensional Dirac points appear away from the Z point. In another work, Xiang *et al.*[36] reported colossal positive magneto-resistance in black phosphorus for P $\geq$ 1.2 GPa and observed a non-trivial π Berry phase from the Shubnikov-de Haas oscillation measurement. These observed changes in black phosphorus at pressure of 1.2 GPa were attributed to an electronic Lifshitz transition[36].

The role of lattice in pressure-induced electronic topological transition has been evident in softening of an acoustic phonon mode at 1.54 GPa in an earlier inelastic neutron scattering experiment[37], where anomalous compressibility and softening of longitudinal ultrasonic wave propagating along c-axis hint the relevance of electron-phonon interaction to pressure induced transitions. High pressure Raman spectroscopy, a sensitive probe of lattice distortion under pressure, has been used in BP up to 13 GPa pressure, displaying changes in the pressure coefficients of Raman frequencies of a few modes as well as appearance of new modes at the structural transitions at $P_{c2} \sim 4.7$ GPa and $P_{c3} \sim 10.5$ GPa[22]. We revisit the high pressure Raman studies in this work with two objectives: (i) to see the Raman signature of electronic topological transition at P_{c1}; (ii) to extend the pressure range to 24 GPa, and (iii) to understand the phonon signatures using first-principles density functional theory (DFT). Our main results are (i) The linewidths of the first order Raman modes go through minimum at the ETT near $P_{c1} \sim$ 1.1 GPa; (ii) Pressure dependence of phonon frequencies and appearance of new modes confirm the two structural transitions at $P_{c2} \sim 4.6$ GPa and $P_{c3} \sim 11$ GPa; (iii) The first order modes B_{2g} and A_g^2 show anomalous softening in the rhombohedral phase; (iv) All the three Raman modes of the orthorhombic structure vanish above $\sim$ 11 GPa in the sc phase; (v) The new modes appearing in the rhombohedra phase show anomalous decrease in frequency with increasing pressure up to 24 GPa; (vi) Using first-principles analysis we show that the transition at the lowest pressure is an electronic topological transition to a phase with a strong Z_2 topology, while the anomalies at higher pressure have a structural origin. We have also identified the symmetry of new modes observed in rhombohedral phase.

II. EXPERIMENTAL DETAILS

Raman measurements were carried out at room temperature in back scattering configuration with micro-optical system equipped with Horiba 800 spectrometer, Peltier-cooled charge controlled detector and 532 nm diode laser. Pressure was generated using a diamond anvil cell (DAC) using 4:1 methanol: ethanol pressure transmitting medium. A thin platelet of dimension $\sim 100\mu m$ cleaved from single crystals of BP, (from M/S Smart Elements) was placed into a stainless steel gasket with sample chamber hole of $\sim 200\mu m$ inserted between the diamonds along with a ruby chip for pressure calibration. Laser power ($< 5mW$) was kept low enough to avoid damage to the sample.

III. COMPUTATIONAL DETAILS

Our first-principles calculations are based on density functional theory (DFT) as implemented in the Quantum ESPRESSO package[38], with the interaction between ionic core and valence electrons modeled with norm-conserving pseudopotentials[39,40]. The exchange-correlation energy of electrons is treated within a generalized gradient approximation (GGA) with a functional form parameterized by Perdew, Burke and Ernzerhof[41]. We use an energy cutoff of 55 Ry to truncate the plane wave basis used in representing Kohn-Sham wave functions, and energy cutoff of 220 Ry for the basis set to represent charge density. Structures are relaxed to minimize energy till the magnitude of Hellman-Feynman force on each atom is less than 0.03 eV/Å. We include van der Waals (vdW) interaction with the parametrization given in Grimme scheme[42]. In self-consistent Kohn-Sham (KS) calculations of configurations of bulk black phosphorous with orthorhombic and rhombohedral unit cell, the Brillouin zone (BZ) integrations were sampled with a uniform mesh of 18x16x16 and 16x16x16 k-points respectively, and 32x32x32 mesh of k-points was used in calculation of electron-phonon coupling of both the structural forms. Phonon spectra and dynamical matrices at Γ-point (q= (0, 0, 0)) as a function of lattice constant (or pressure) were determined using density functional linear response as implemented in Quantum ESPRESSO(QE)[38], which employs the Green's function method to avoid explicit calculations of unoccupied Khon-Sham states. Since DFT typically underestimates the electronic bandgap, we have used HSE functional[43] to estimate the gaps accurately, with the mixing parameter of 0.25 and reciprocal space integration sampled on a 4x4x4 mesh of k-points.

Z_2 topological invariants can be defined using the notion of time reversal polarization[44,45] derived in terms of hybrid Wannier charge centres (WCCs)[46]. In a time-reversal invariant system, electronic bands always come in time-revsersed pairs (let's say I & II denote such pairs). Then the Z_2 invariant in a time-reversal invaraint plane is given by[44],

$$(\sum_n [\bar{x}_n^I(T/2) - \bar{x}_n^{II}(T/2)] - \sum_n [\bar{x}_n^I(0) - \bar{x}_n^{II}(0)])\ mod\ 2, \quad (1)$$

where $\bar{x}_n = \frac{i}{2\pi}\int_{-\pi}^{\pi} dk < u_{nk}|\frac{\partial}{\partial_k}|u_{nk} >$ is the Wannier charge center calculated at t=0 and t=T/2 planes which are invariant under time reversal symmetry, where T represents the period of a full cyclic adiabatic evolution. In the Brillouin zone of a periodic crystal T is equivalent to a reciprocal lattice vector which defines the periodicity in the reciprocal space. The topological invariant of a plane is non-zero if the WCCs switch pairs under an adiabatic evolution in the half-cycle, which can be easily tracked by seeing evolution of the mid-point of the largest gap (as marked by blur rhombus in Fig. 7) between two adjacent WCCs with t ∈ [0, T/2] in the half-cycle[44]. In this case, the rhombuses exhibits abrupt jumps in their half-cyclic evolution and cross odd number of WCCs[44]. We have calculated the strong topological index (ν_0) by taking the sum (modulo 2) of the topological invariants calculated at k_z=0 and k_z=0.5 planes in the Brillouin zone of black phosphorous using Z2Pack code[47]. At each of these planes, WCC, calculated along k_x direction, evolve along the k_y direction (parameterized with time, t).

IV. RESULTS AND DISCUSSION

A. Experimental Results

The unit cell of BP contains 4 atoms which gives 12 normal modes. According to factor group analysis, at ambient pressure the Brillouin zone center point phonon modes are $2A_g+B_{1g}+B_{2g}+2B_{3g}+A_u+2B_{1u}+2B_{2u}+B_{3u}$: out of which $2A_g$, B_{1g}, B_{2g} and $2B_{3g}$ are Raman active. Experimentally three Raman modes A_g^1, B_{2g} and A_g^2 were observed at 360, 438 and 460 cm^{-1} respectively as shown in lower panel of Fig. 2. The other two previously reported[22] Raman modes B_{1g} (192 cm^{-1}) and B_{3g}^1 (227 cm^{-1}) are very weak and difficult to separate from the background. The phosphorus atoms vibrate along the out of plane (z) for the A_g^1 (360 cm^{-1}) mode, along armchair (y) for the B_{2g} (438 cm^{-1}) mode and zig zag (x) directions for the A_g^2 (460 cm^{-1}) mode. Fig. 2 shows the pressure evolution of the Raman spectra of BP at a few representative pressures. The Lorentzian line shapes are used to fit the Raman spectra at different pressures to obtain phonon frequencies and full width at half maximum (FWHM). Fig. 3 shows the pressure dependence of phonon frequencies. The solid blue lines are the linear fit to the experimental data points. The vertical dashed red lines indicate two structural phase transition from orthorhombic to rhombohedral and from rhombohedral to simple cubic phase. From Fig. 2, it cam be seen that the intensities of A_g^1, B_{2g} and A_g^2 Raman modes of the orthorhombic structure decreases gradually with pressure and disappeared completely at 11 GPa. Further, two

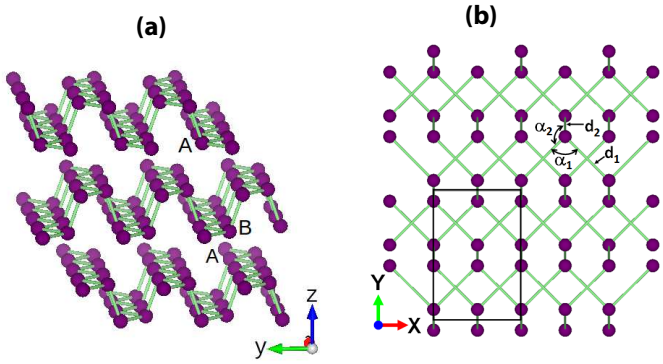

FIG. 1: Side (a) and top (b) views of the layered structure of bulk black phosphorous. d_1 and d_2 are the P-P bonds lengths. d_1 is the distance between two P atoms in a plane while d_2 is the nearest neighbor distance. α_1 is the bond angle between two d_1's and the bond angle between d_1 and d_1 is α_2.

new Raman modes labelled as N1 and N2 at 240 and 300 cm^{-1} respectively, emerged at 4.6 GPa and remain till 24 GPa. Another new mode labelled as N3 at 370 cm^{-1} arises at 7.4 GPa and diminishes at 15.9 GPa.

Fig. 3 shows that the frequencies of A_g^1, B_{2g} and A_g^2 modes show increase with pressure in orthorhombic phase. The slope for the A_g^1 (S=dω/dP) is more as compared to that for the B_{2g} and A_g^2 modes. Noting that the eigen vectors of the A_g^1 mode are perpendicular to the puckered layers, larger pressure derivative of frequency (S) signifies that van der Waals bond can be greatly compressed. Fig. 3 also shows that all the three modes of the orthorhombic phase (A_g^1, B_{2g} and A_g^2) persist even beyond 4.6 GPa. This can be due to two possibilities (i) that the orthorhombic to rhombohedral transformation is completed only at ∼ 11 GPa; (ii) the Raman active modes of the rhombohedral phase are at the frequencies close to the values in the orthorhombic phase. The latter possibility is ruled out as there are only two Raman active modes in rhombohedral phase (to be discussed latter) whose frequencies are not close to the above three modes. In rhombohedral phase at 7.4 GPa, A_g^2 and B_{2g} modes soften anomalously (the effect is more for B_{2g} mode). Further Fig. 3 shows that the Raman modes N1, N2 and N3 show anomalous softening with pressure in rhombohedral as well as in simple cubic phase. It is clear from Fig. 3 that the slope S for the N3 mode is more than N1 and N2 modes. Fig. 4(a) shows the effect of pressure on FWHM of the Raman modes. The range from 0 to 4 GPa has been magnified in Fig. 4(b). The solid blue lines are the linear fit. It is clear from Fig. 4(b) that the FWHM of all the three Raman modes show a minimum at 1.1 GPa which coincide with the ETT transition pressure. We now present our theoretical calculations to understand the anomalies in phonon spectra with pressure observed in the experiments.

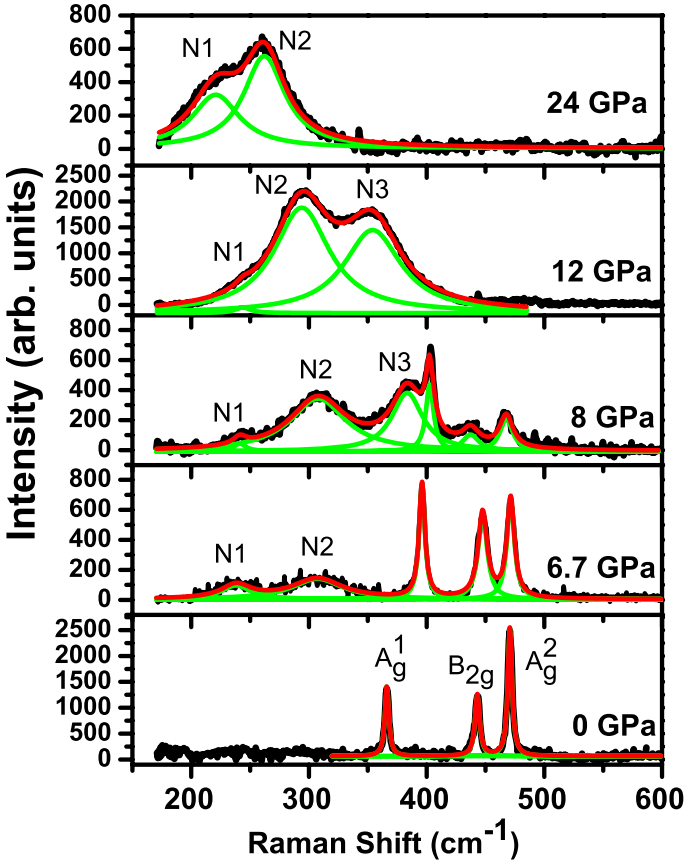

FIG. 2: Pressure evolution of Raman spectra. The solid lines (red and green) are the Lorentzian fits to the experimental data (black). N1, N2 and N3 are the new modes.

B. Theoretical calculations

1. *Low Pressure Transition*

Our optimized structural parameters of orthorhombic structure, a, b, c, d_1, d_2, α_1 and α_2 are 4.42Å, 3.32Å, 10.46Å, 2.224 Å, 2.244 Å, 96.34° and 102.09° respectively, in good agreement with the experimental values[48]. Here d_1 is the bond length of in-plane P atoms, d_2 defines the distance out-of-plane P atoms; α_2 and α_1 are the bond angles between d_1 and d_2, and the two d_1 bonds respectively (see Fig. 1(b)). BP is a semiconductor with a gap of 0.33 eV at Z-point (0.0, 0.0, 0.5) as estimated with HSE functional (Fig. 5(a)), which is in good agreement with the experiment ($E_g = 0.35$ eV). We note that there is no band gap in the structure at 0 GPa calculated with GGA functional based theory (Fig. 5(b)).

Our calculated frequencies of A_g^1, B_{2g} and A_g^2 modes using GGA functionals are 453 cm^{-1}, 418 cm^{-1} and 354 cm^{-1}, which agree well with the observed frequencies (460cm^{-1}, 438cm^{-1} and 360cm^{-1}) of these modes. Raman experiments (Fig. 4(b)) showed non-monotonic dependence of FWHM of A_g^1, B_{2g} and A_g^2 modes on pressure, displaying a minimum at 1.1 GPa. Since the anomalous change in FWHM can be an indicator of electronic topological transition (ETT)[32], and given the experimental observations of Xiang et al.[36] and theoretical study of Gong et al.[35], we first studied electronic structure of black phosphorus as a function of hydrostatic pressure using highly accurate HSE calculations. Our calculations show that the band inversion occurs at Z point between $P = 0.25$ and $P = 0.50$ GPa (Fig. 6) following which the band gap opens up above $P \geq 0.5$ GPa (Fig. 5(c)), which is in contrast to the earlier DFT study (within GGA and mBJ functional) where persistence of robust band crossing is reported after band inversion[35]. Based on the HSE calculations, our estimate of the transition pressure is P $\sim$ 0.5 GPa, in reasonable agreement with theoretically predicted transition pressure (P $\sim$ 0.6 GPa) by Ruixiang *et. al*[49], and also close to the pressure of observed Raman anomalies (P_{c1} $\sim$1.1 GPa).

Although earlier studies[35,36] reported pressure induced electronic topological transition (Lifshitz transition) in black phosphorus following band inversion near P = 1.2 GPa, the nature of electronic topology has not been clearly elucidated. To investigate the electronic topology of black phosphorus, we determined the Z_2 topological invariant (ν_0) as a function of pressure (Fig. 7). The evolution of hybrid Wannier charge centers (WCCs) along k_y-direction is marked by circle while their largest gap function is marked by blue rhombus for k_z =0 plane and k_z=0.5 plane. It is clear from Fig. 7 a,b that for P <0.5 GPa both $k_z = 0$ and k_z=0.5 planes are topologically trivial as Z_2 invariants for both the planes are zero, and hence strong topological index ν_0=0. However, at P >0.5 GPa (Fig. 7 c,d), Z_2 invaraint for $k_z = 0$ plane is 1, as evident from the discontinuous jump of the gap function along k_y, whereas Z_2 invaraint is zero for k_z=0.5 plane, and hence the strong topological index ν_0 of the state at this pressure is 1. Thus we find that $\nu_0 = 0$ for $P < 0.5$ GPa, whereas $\nu_0 = 1$ for $P \geq 0.5$ GPa signifying Z_2 topological insulating nature of black phosphorus above 0.5 GPa. Thus, the minimum in FWHM of Raman active modes at (P_{c1}) is correlated with the pressure induced electronic topological phase transition. The observation of non-trivial π Berry phase and colossal magnetoresistance for P > 1.2 GPa in experiment[36] are also consistent with our finding that the BP becomes topologically non-trivial for P > 0.5 GPa. The discrepancy between our calculated transition pressure (0.5 GPa) and previously reported ones (1.2 GPa) falls within the typical errors of DFT calculations.

We further examine the minimum in the FWHM (at P_{c1}) which is related to the electron phonon coupling constant λ. This calculation is not straight-forward with HSE functionals and hence were done using GGA functionals. Fig. 4 (c) shows the dependence of λ of the three Raman modes on pressure between -2 GPa to 1 GPa. We have gone to negative pressure because GGA functionals calculations show semiconductor to semi-metal transition at P_{c1} = -1.5 GPa (Fig. 5(d)). This discrepancy in P_{c1} using GGA functionals as compared to experiment (P_{c1}

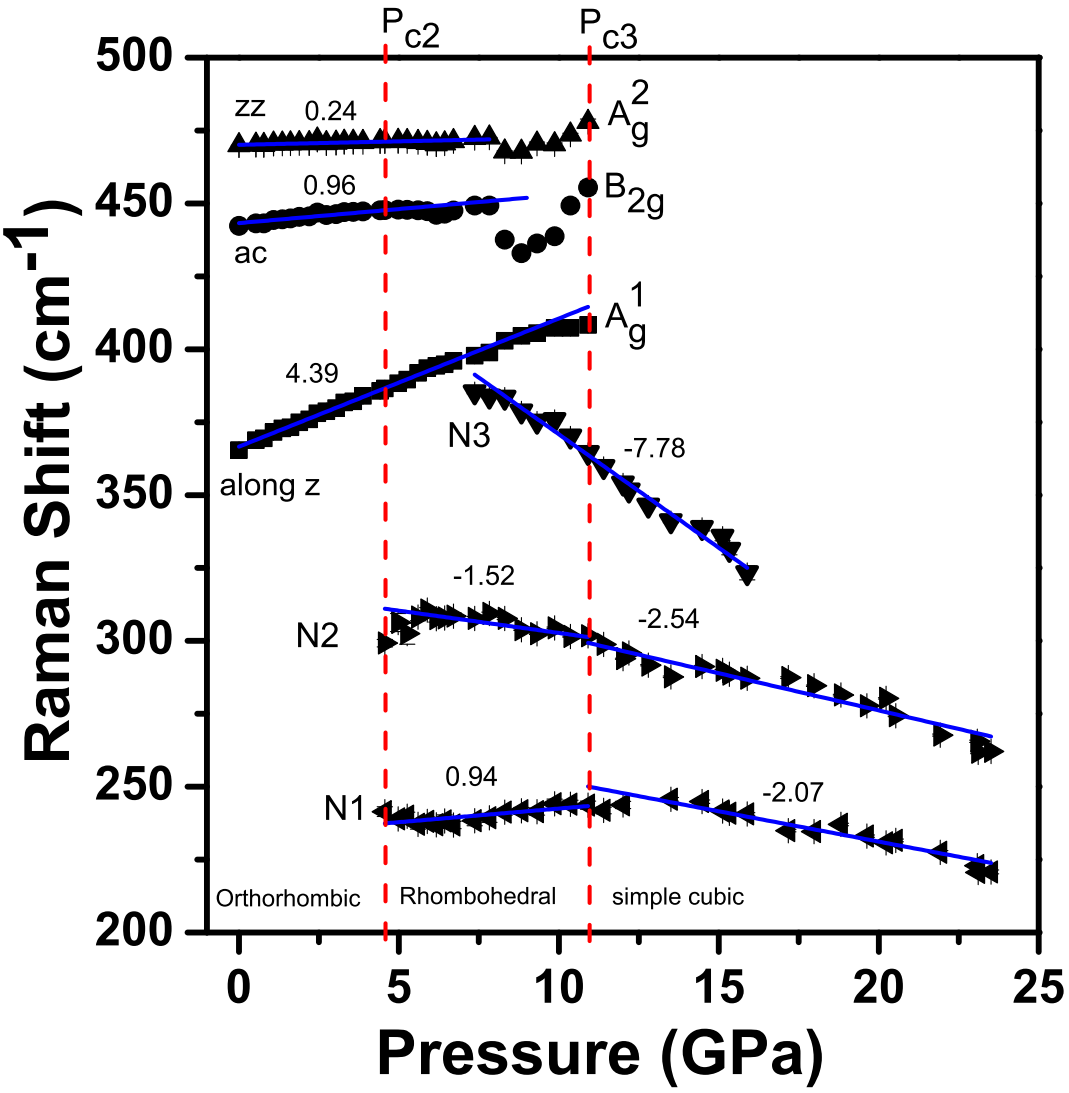

FIG. 3: Pressure dependence of phonon frequencies. The vertical dashed lines indicate the two structural phase transition pressures. The solid blue lines are the linear fit. The slope dω/dP in units of cm^{-1} /GPa is given near the lines.

= 1.1 GPa) and HSE functionals (P_{c1} = 0.5 GPa) points to the inadequacy of the GGA functionals in predicting the transition pressure. Fig. 4 (c) reveals that the λ does show a shallow minimum at P_{c1} = -1.5 GPa for the A_g^1 and A_g^2 modes. We did not see any anomaly in the λ of B_{2g} mode with pressure.

2. *Anomalies at High Pressure Transitions: Structural Origin*

We now address the pressure dependence of A_g^1, A_g^2 and B_{2g} modes of the orthorhombic phase. The calculated frequencies of the orthorhombic phase as a function of pressure (shown in the Fig. 8) clearly display that the frequencies of A_g^1 and A_g^2 modes harden up to $\sim$ 3 GPa. Interestingly, the frequency of B_{2g} and A_g^2 modes show softening at high pressure; resembling with the anonmalous pressure dependence of the B_{2g} and A_g^2 modes seen in the experiments between 7 and 9 GPa (Fig. 3). To correlate the softening of the B_{2g} and A_g^2 modes with structural modifications, we examine the pressure dependence of the internal parameters d_1, d_2, α_1 and α_2 (see Fig. 1 for description).

Atomic vibrations of the A_g^1 mode (Fig. 8) involve stretching of the d_2 bond. From the variation in d_2 bond

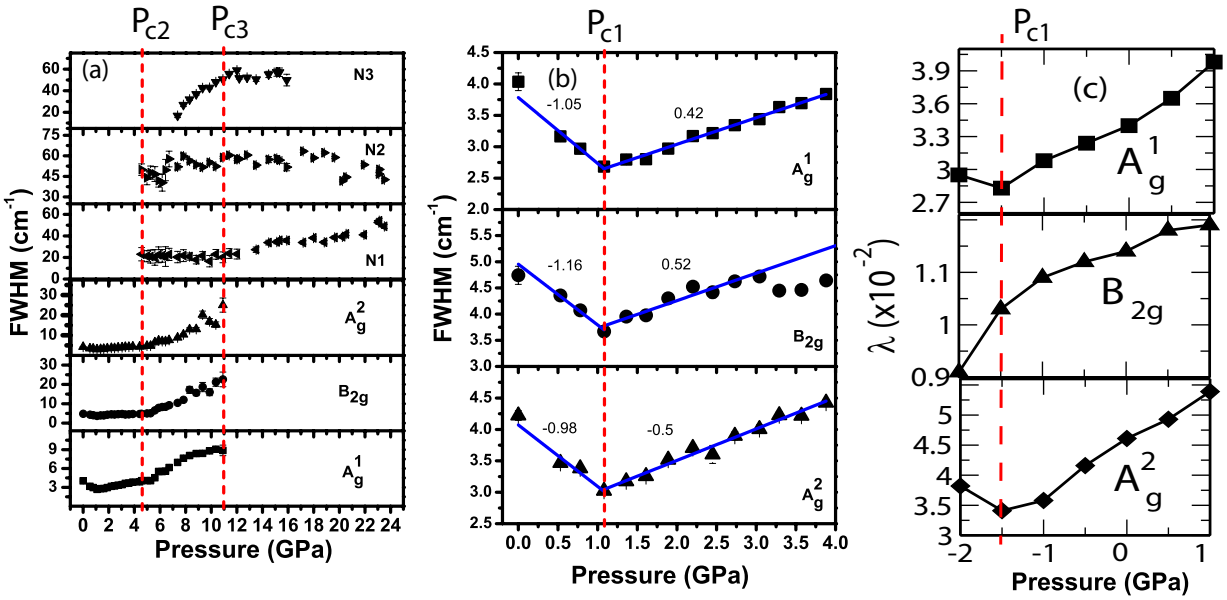

FIG. 4: (a) Pressure evolution of FWHM of Raman modes. The vertical dashed lines indicate the two structural phase transition pressures. (b) Magnified plot FWHM in the pressure range 0 to 4 GPa. The vertical dashed line indicates the semiconductor to topological insulator phase transition pressures. The solid blue lines are linear fit. The slope dω/dP in units of cm^{-1} /GPa is given near the lines. (c) Variation in the calculated electron-phonon coupling of Raman active modes A_g^1, B_{2g} and A_g^2 of BP with pressure in orthorhombic phase. The vertical dashed line indicates the semiconductor to topological insulator phase transition pressures.

with pressure (Fig. 9(a)), we find that d_2 decreases monotonically with pressure and the Δd_2 is ~ 0.04 Å up to 10 GPa. As a result, A_g^1 hardens with pressure. The atomic vibrations of the B_{2g} mode (Fig. 8) affects bond angle α_2, which decreases with increasing pressure (Fig. 9(b)), similar to the frequency of B_{2g} mode. Atomic displacements of the A_g^2 mode (Fig. 8) involve stretching of the d_1 bond. Fig. 9(a) shows that d_1 decreases with pressure upto 3 GPa, and starts increasing from 3-6 GPa, and subsequently decreases with pressure upto 12 GPa. In this case, the change in d_1 with pressure is much smaller than that in d_2, which is also reflected in softening of B_{2g} and A_g^2 modes. As a result of variation of d_1 with pressure, the A_g^2 mode softens with pressure and this softening is less than the softening of the B_{2g} mode.

The space group of BP in rhombohedral structure (also known as A7 phase after 4.6 GPa) is $R\bar{3}m$ with primitive cell containing 2 atoms. Group theory gives zone center optical modes as A_{1g}+E_g+A_{2u}+E_u, where A_{1g} and E_g are the Raman active modes and A_{2u} and E_u are infrared active modes. The frequencies of the A_{1g} and E_g modes are 350 cm^{-1} and 255 cm^{-1} at 4 GPa. We identify the experimentally observed N3 mode as A_{1g} mode and N1 as the E_g mode. We are unable to assign the experimentally observed N2 mode (300 cm^{-1}). From first-principles calculations, the rhombohedral structure is stable from 4 GPa to 12 GPa and, unstable modes appear in phonon dispersion beyond this pressure. The pressure dependence of phonon frequencies and electron phonon coupling λ of A_{1g} and E_g modes are shown in Fig. 10. It is clear from Fig. 10 that A_{1g} and E_g modes soften and broaden with increasing pressure, which is consistent with softening and broadening of N3 and N1 modes observed in experiment (Fig. 3).

V. CONCLUSION

High pressure Raman study of BP up to 24 GPa is reported using diamond anvil cell under hydrostatic conditions. The line width of all the three Raman modes A_g^1, B_{2g} and A_g^2 of the orthorhombic phase decrease with pressure up to 1.1 GPa and then increase, thus showing a minimum at ~ 1.1 GPa corresponding to the transition pressure of ETT. Using first-principles calculations, we find that the low pressure phase transition in BP is a semiconductor to topological insulator transition. Our calculations of the Z_2 invariant confirm the change in electronic topology marking a transition from band to topological insulating state. The Raman shift of these modes show normal hardening with pressure in orthorhombic phase. B_{2g} and A_g^2 modes show anomalous softening in rhombohedral phase at 7.4 GPa while A_g^1 mode exhibits normal hardening. These modes disappear completely at 11 GPa in the sc phase. The new modes N1, N2 and N3 arising in rhombohedral phase also show anomalous softening of the frequency with pressure. We uncover the origin of these anomalous softening of Raman modes in the variation of internal structural parameters with pressure, and identify the symmetry of the new modes appearing upon

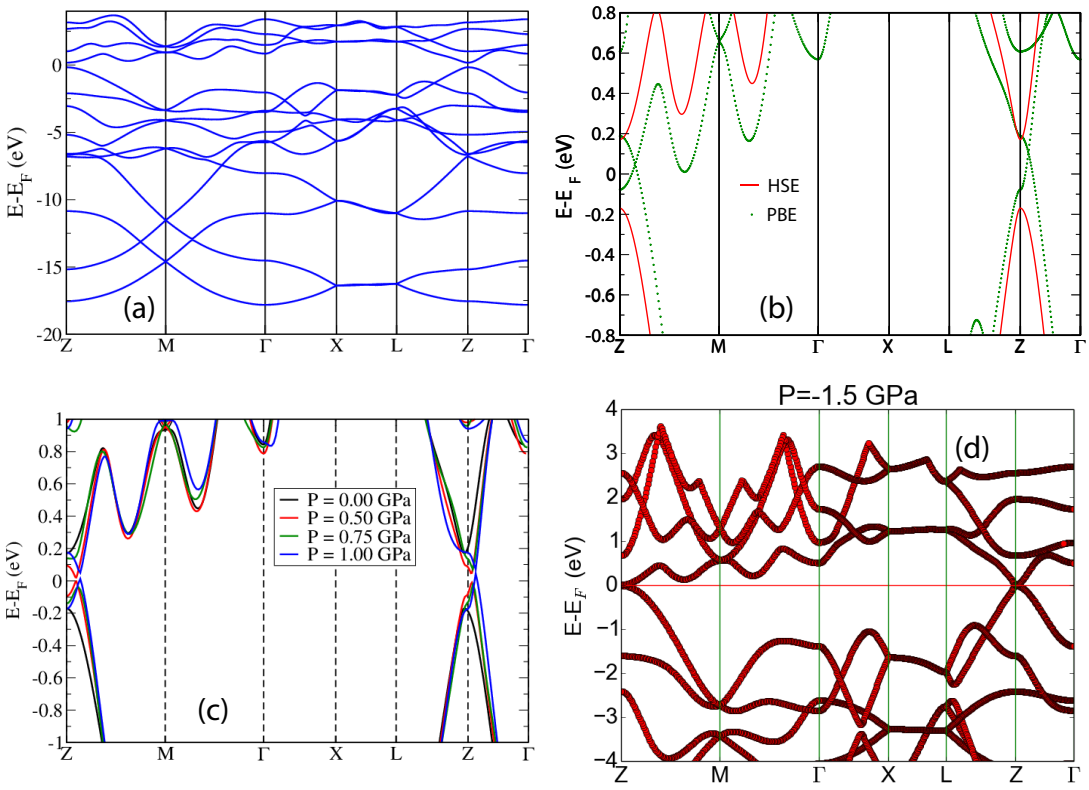

FIG. 5: Electronic structure of BP in orthorhombic phase. (a) Electronic structure of BP at $P = 0$ GPa calculated with HSE functionals. Note that we used Wannier functions[50] to plot band structure with HSE functionals. (b) Comparison of electronic structure near the gap obtained with HSE and PBE functionals at $P = 0$ GPa. BP exhibit a gap of 0.33 eV at Z-point, which is captured correctly with HSE functionals whereas PBE calculations gives no gap. (c) Electronic structure near the gap obtained with HSE functionals at different pressures. (d) Electronic structure of BP calculated with PBE functional at P= -1.5 GPa. At P = -2 GPa, calculations with PBE functionals show a gap which closes at P=-1.5GPa.

pressure in experiments.

AKS and UVW thanks DST for the JC Bose fellowship. AKS thanks DST Nanomission for the financial support.

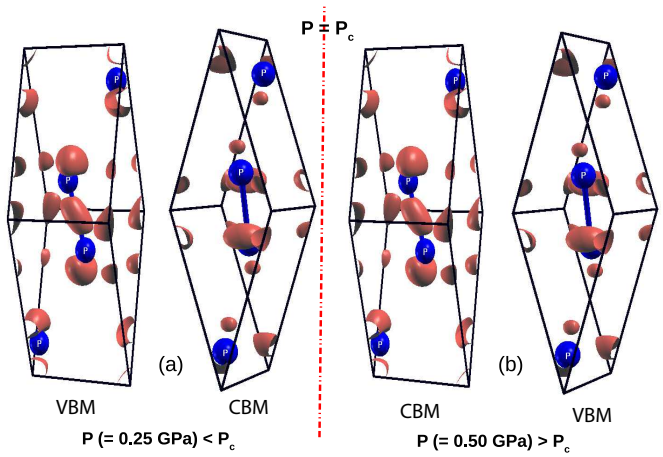

FIG. 6: Band inversion during pressure induced electronic topological transition (ETT) in BP. Isosurfaces of charge densities associated with electronic states at valance band maximum (VBM) and conduction band minimum (CBM) at Γ-point (a) before and (b) after the ETT revealing band inversion across this transition.

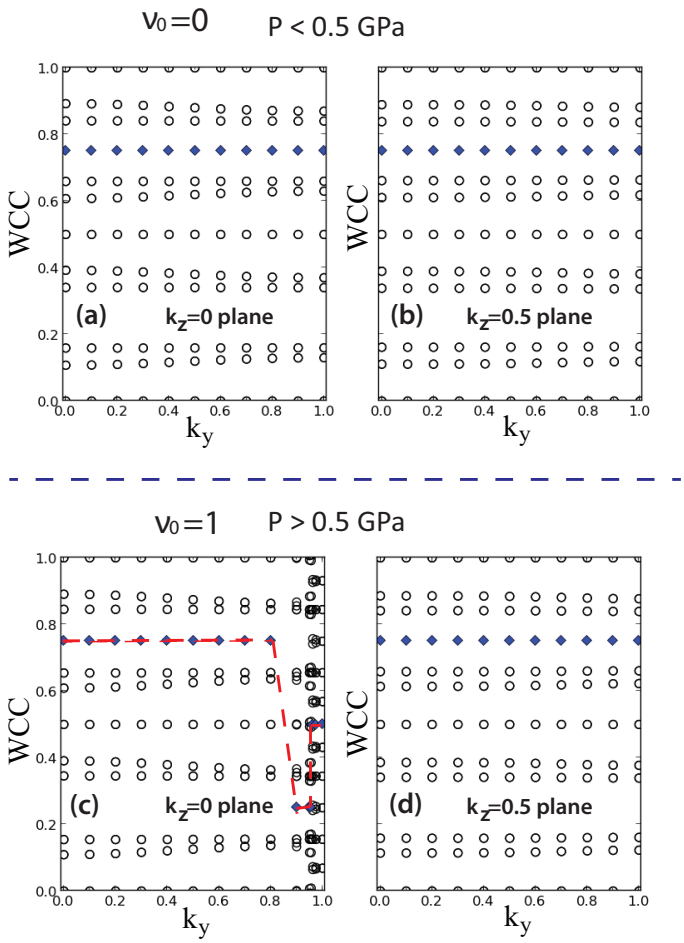

FIG. 7: Calculation of Z_2 topological index (ν_0) before (P <0.5 GPa) and after (P >0.5 GPa GPa) the phase transition. Evolution of hybrid Wannier charge centers (WCCs) along k_y-direction (marked by circle) and their largest gap function (blue rhombus) for (a) k_z =0 plane and (b) k_z=0.5 plane. It is clear that both k_z = 0 and k_z=0.5 planes are topologically trivial as Z_2 invariants for both the planes are zero, hence strong topological index ν_0=0. At P >0.5 GPa, Z_2 invaraint for k_z = 0 plane is 1, as evident from the discontinuous jump (indicated by red dotted line) of the gap function along k_y (c), whereas Z_2 invaraint is zero for k_z=0.5 plane (d), hence the strong topological index ν_0 at this pressure is 1.

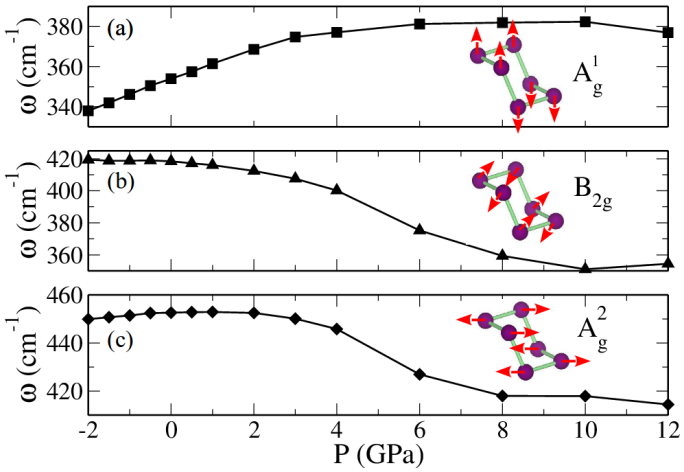

FIG. 8: Change in the frequencies of Raman active modes (a) A_g^1, (b) B_{2g} and (c) A_g^2 modes of BP in orthorhombic phase with pressure. Insets of (a), (b) and (c) show atomic displacements in these Raman active modes.

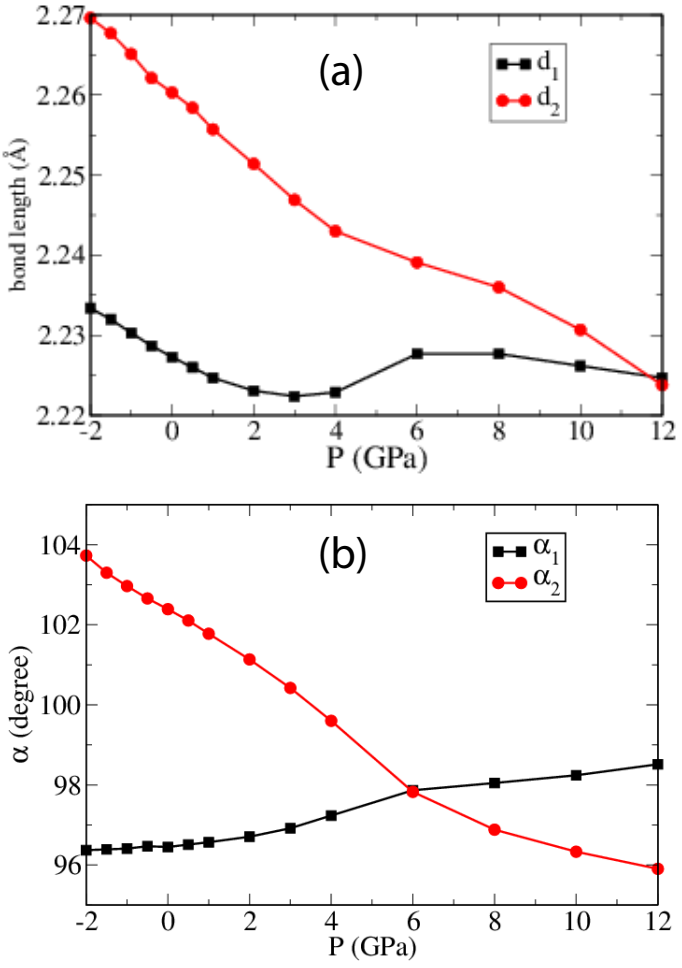

FIG. 9: Evolution of bond lengths (a) and bond angles (b) of BP in orthorhombic phase with pressure.

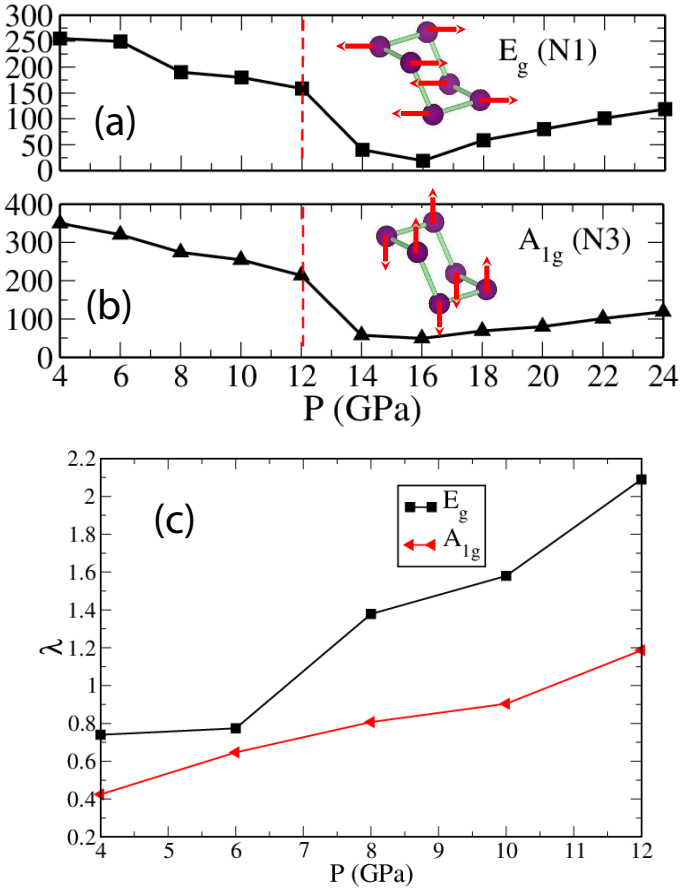

FIG. 10: Change in the calculated frequencies of Raman active modes with pressure of BP in rhombohedral phase, (a) E_g mode and (b) A_{1g} mode (Insets of (a) and (b) showing their atomic displacements). Note that N1 and N3 are the modes observed in experiments. The vertical dashed red line indicates the pressure till which rhombohedral phase is stable. (c) Change in electron-phonon coupling of Raman active modes E_g and A_{1g} of BP in rhombohedral phase.

* To whom correspondence should be addressed; Electronic address: asood@physics.iisc.ernet.in

[1] X. Ling, H. Wang, S. Huang, F. Xia, and M. S. Dresselhaus, Proc. Natl. Acad. Sci. **112**, 4523 (2015).
[2] B. Chakraborty, S. N. Gupta, A. Singh, M. Kuiri, C. Kumar, D. Muthu, A. Das, U. Waghmare, and A. Sood, 2D Materials **3**, 015008 (2016).
[3] L. Li, Y. Yu, G. J. Ye, Q. Ge, X. Ou, H. Wu, D. Feng, X. H. Chen, and Y. Zhang, Nat. Nanotechnol. **9**, 372 (2014).
[4] F. Xia, H. Wang, and Y. Jia, Nature commun. **5** (2014).
[5] H. Liu, A. T. Neal, Z. Zhu, Z. Luo, X. Xu, D. Tománek, and P. D. Ye, ACS Nano **8**, 4033 (2014).
[6] S. P. Koenig, R. A. Doganov, H. Schmidt, A. C. Neto, and B. Oezyilmaz, App. Phys. Lett. **104**, 103106 (2014).
[7] A. Rodin, A. Carvalho, and A. C. Neto, Phys. Rev. lett. **112**, 176801 (2014).
[8] J. Qiao, X. Kong, Z.-X. Hu, F. Yang, and W. Ji, Nature Commun. **5** (2014).
[9] S. Zhang, J. Yang, R. Xu, F. Wang, W. Li, M. Ghufran, Y.-W. Zhang, Z. Yu, G. Zhang, Q. Qin, et al., ACS Nano **8**, 9590 (2014).
[10] K. Novoselov, A. K. Geim, S. Morozov, D. Jiang, M. Katsnelson, I. Grigorieva, S. Dubonos, and A. Firsov, Nature **438**, 197 (2005).
[11] Y. Zhang, Y.-W. Tan, H. L. Stormer, and P. Kim, Nature **438**, 201 (2005).
[12] K. F. Mak, C. Lee, J. Hone, J. Shan, and T. F. Heinz, Phys. Rev. lett. **105**, 136805 (2010).
[13] A. Splendiani, L. Sun, Y. Zhang, T. Li, J. Kim, C.-Y. Chim, G. Galli, and F. Wang, Nano Lett. **10**, 1271 (2010).
[14] A. M. Jones, H. Yu, J. S. Ross, P. Klement, N. J. Ghimire, J. Yan, D. G. Mandrus, W. Yao, and X. Xu, Nature Phys. **10**, 130 (2014).
[15] H. Liu, Y. Du, Y. Deng, and D. Y. Peide, Chem. Soc. Rev. **44**, 2732 (2015).
[16] J. C. Jamieson, Science **139**, 1291 (1963).
[17] L. Cartz, S. Srinivasa, R. Riedner, J. Jorgensen, and T. Worlton, J. Chem. Phys. **71**, 1718 (1979).
[18] T. Kikegawa and H. Iwasaki, Acta Crystallogr. Sect. B **39**, 158 (1983).
[19] J. K. Burdett and S. Lee, J. Solid State Chem. **44**, 415 (1982).
[20] S. Sugai, T. Ueda, and K. Murase, J. Phys. Soc. Jpn. **50**, 3356 (1981).
[21] C. Vanderborgh and D. Schiferl, Phys.l Rev. B **40**, 9595 (1989).
[22] Y. Akahama, M. Kobayashi, and H. Kawamura, Solid state commun. **104**, 311 (1997).
[23] Y. Akahama, M. Kobayashi, and H. Kawamura, Phys.Rev. B **59**, 8520 (1999).
[24] Y. Akahama, H. Kawamura, S. Carlson, T. Le Bihan, and D. Häusermann, Phys.l Rev. B **61**, 3139 (2000).
[25] J. Wittig and B. Matthias, Science **160**, 994 (1968).
[26] H. Kawamura, I. Shirotani, and K. Tachikawa, Solid state commun. **49**, 879 (1984).
[27] K. Ito and S. Endo, Solid State Commun. **36**, 701 (1980).
[28] M. Okajima, S. Endo, Y. Akahama, and S.-i. Narita, Jpn. J. Appl. Phys. **23**, 15 (1984).
[29] Y. Akahama, S. Endo, and S. Narita, Physica B+ C **139**, 397 (1986).
[30] P.-L. Gong, D.-Y. Liu, K.-S. Yan, Z.-J. Xiang, X.-H. Chen, S.-Q. Shen, and L.-J. Zou, arXiv preprint arXiv:1507.03213 (2015).
[31] Z. J. Xiang, G. J. Ye, C. Shang, B. Lei, N. Z. Wang, K. S. Yang, D. Y. Liu, F. B. Meng, X. G. Luo, L. J. Zou, et al., Phys. Rev. Lett. **115**, 186403 (2015).
[32] A. Bera, K. Pal, D. V. S. Muthu, S. Sen, P. Guptasarma, U. V. Waghmare, and A. K. Sood, Phys. Rev. Lett. **110**, 107401 (2013).
[33] K. Pal and U. V. Waghmare, Appl. Phys. Lett. **105**, 062105 (2014).
[34] X. Xi, C. Ma, Z. Liu, Z. Chen, W. Ku, H. Berger, C. Martin, D. B. Tanner, and G. L. Carr, Phys. Rev. Lett. **111**, 155701 (2013).
[35] P.-L. Gong, D.-Y. Liu, K.-S. Yang, Z.-J. Xiang, X.-H. Chen, Z. Zeng, S.-Q. Shen, and L.-J. Zou, Phys. Rev. B **93**, 195434 (2016).
[36] Z. J. Xiang, G. J. Ye, C. Shang, B. Lei, N. Z. Wang, K. S. Yang, D. Y. Liu, F. B. Meng, X. G. Luo, L. J. Zou, et al., Phys. Rev. Lett. **115**, 186403 (2015).
[37] Y. Yamada, Y. Fujii, Y. Akahama, S. Endo, S. Narita, J. D. Axe, and D. B. McWhan, Phys. Rev. B **30**, 2410 (1984).
[38] P. Giannozzi, S. Baroni, N. Bonini, M. Calandra, R. Car, C. Cavazzoni, D. Ceresoli, G. L. Chiarotti, M. Cococcioni, I. Dabo, et al., J. Phys. Condens. Matter **21**, 395502 (2009).
[39] S. Goedecker, M. Teter, and J. Hutter, Phys. Rev. B **54**, 1703 (1996).
[40] C. Hartwigsen, S. Goedecker, and J. Hutter, Phys. Rev. B **58**, 3641 (1998).
[41] J. P. Perdew, K. Burke, and M. Ernzerhof, Phys. Rev. Lett. **77**, 3865 (1996).
[42] S. Grimme, J. Comput. Chem. **25**, 1463 (2004).
[43] J. Heyd, G. E. Scuseria, and M. Ernzerhof, J. Chem. Phys. **118**, 8207 (2003).
[44] A. A. Soluyanov and D. Vanderbilt, Phys. Rev. B **83**, 235401 (2011).
[45] J. Bhattacharjee and U. V. Waghmare, Phys. Rev. B **71**, 045106 (2005).
[46] L. Fu and C. L. Kane, Phys. Rev. B **74**, 195312 (2006).
[47] D. Gresch, O. Y. G. Autés, . T. M, D. Vanderbilt, B. A. Bernevig, and A. A. Soluyanov, arXiv:1610.08983v1 (2016).
[48] Y. Takao and A. Morita, Physica B+C **105**, 93 (1981).
[49] R. Fei, V. Tran, and L. Yang, Phys. Rev. B **91**, 195319 (2015).
[50] A. A. Mostofi, J. R. Yates, G. Pizzi, Y.-S. Lee, I. Souza, D. Vanderbilt, and N. Marzari, Comput. Phys. Commun. **185**, 2309 (2014).